Pergamon

0020-7225(95)00058-5

Int. J. Engng Sci. Vol. 34, No. 1, pp. 113–124, 1996

0020-7225/96 $15.00 + 0.00

THE BLASIUS BOUNDARY-LAYER FLOW OF A MICROPOLAR FLUID

D. A. S. REES
School of Mechanical Engineering, University of Bath, Claverton Down, Bath BA2 7AY, England

ANDREW P. BASSOM†
School of Mathematics, University of New South Wales, P.O. Box 1, Kensington, New South Wales 2033, Australia

Abstract—We consider the Blasius boundary-layer flow of a micropolar fluid over a flat plate. Due to inadequacies in previous studies a full derivation of the boundary-layer equations is given. The resulting nonsimilar equations are solved using the Keller-box method and solutions for a range of parameters are presented. It is found that a two-layer structure develops as the distance downstream increases. An asymptotic analysis of this structure is presented, and the agreement between the analysis and the numerical solution is found to be excellent.

1. INTRODUCTION

A micropolar fluid is one which contains suspensions of rigid particles such as blood, liquid crystals, dirty oil and certain colloidal fluids, and which exhibits a microstructure. The theory of such fluids was first formulated by Eringen [1] and has very recently been applied to a wide range of classical flows. For example, Gorla [2–4] and Arafa and Gorla [5] have considered the free and mixed convection flow of a micropolar fluid from flat surfaces and cylinders, and the effect of stationary surface waves on free convection from a vertically aligned heated surface has been investigated by Chiu and Chou [6].

Of more interest to the present work are the papers by Unsworth and Chiam [7] and Ahmadi [8]; these authors, independently, have studied the micropolar analogue of the Blasius boundary layer (although it should be noted that the analysis of [7] was for the more general configuration of flow past a wedge). Their respective results, where they can be compared, do not agree because the initial assertions are at variance. For example, in [7], it is assumed that the microrotation vector is zero on a solid surface, whereas in [8] it is proportional to the fluid shear stress, a result which is now generally accepted as being more realistic. A second major difference between the papers lies in the fact that the microinertia density is assumed to be a constant in [7], but is allowed to vary in [8]. Unfortunately, the insistence in [8] that the flow should be self-similar leads to the unphysical result that the microinertia density varies as the square of the perpendicular distance from the surface once outside the boundary layer. Clearly a re-examination of this fundamental flow is in order, and this motivates the present paper.

We derive and solve the full boundary layer equations for the Blasius boundary-layer flow of a micropolar fluid over a flat plate. The resulting equations are different from those of both Unsworth and Chiam [7] and Ahmadi [8]. Detailed numerical results are presented, as is an asymptotic analysis for large distances from the leading edge; such an analysis is necessary because the numerical results indicate that the boundary layer develops a two-layer structure at sufficiently large distances from the leading edge. Following [4] we consider a variable ratio of gyration component and fluid shear stress at a solid boundary; when this ratio is exactly $\frac{1}{2}$ we demonstrate that there is a similarity solution and no two-layer structure forms.

†Permanent address: Department of Mathematics, University of Exeter, North Park Road, Exeter EX4 4QE, England.

2. GOVERNING EQUATIONS

The full equations governing the isothermal two-dimensional flow of a micropolar fluid are,

$$\bar{u}_{\bar{x}} + \bar{v}_{\bar{y}} = 0, \tag{1}$$

$$\rho(\bar{u}_{\bar{t}} + \bar{u}\bar{u}_{\bar{x}} + \bar{v}\bar{v}_{\bar{y}}) = -\bar{p}_{\bar{x}} + (\mu + \kappa)(\bar{u}_{\bar{x}\bar{x}} + \bar{u}_{\bar{y}\bar{y}}) + \kappa\bar{N}_{\bar{y}}, \tag{2}$$

$$\rho(\bar{v}_{\bar{t}} + \bar{u}\bar{v}_{\bar{x}} + \bar{v}\bar{v}_{\bar{y}}) = -\bar{p}_{\bar{y}} + (\mu + \kappa)(\bar{v}_{\bar{x}\bar{x}} + \bar{v}_{\bar{y}\bar{y}}) - \kappa\bar{N}_{\bar{x}}, \tag{3}$$

$$\rho j(\bar{N}_{\bar{t}} + \bar{u}\bar{N}_{\bar{x}} + \bar{n}\bar{N}_{\bar{y}}) = -2\kappa\bar{N} + \kappa(\bar{v}_{\bar{x}} - \bar{u}_{\bar{y}}) + \operatorname{div}(\gamma\nabla\bar{N}), \tag{4}$$

$$j_{\bar{t}} + \bar{u}j_{\bar{x}} + \bar{v}j_{\bar{j}} = 0 \tag{5}$$

(see Ahmadi [8]). Here, $(\bar{x}, \bar{y})$ are the coordinates parallel with and perpendicular to the flat surface, $(\bar{u}, \bar{v})$ is the velocity vector, $\bar{p}$ the pressure, $\bar{N}$ the component of the gyration vector normal to the x–y plane, and j is the microinertia density. Further, ρ is the fluid density, μ the viscosity, κ the micrototation parameter (also known as the coefficient of gyroviscosity in [9] and as the vortex viscosity in [6] and [10]), and γ is the spin-gradient viscosity given by $\gamma = (\mu + \kappa/2)j$ (see [8]). We follow the work of many recent authors by assuming that j is a constant and therefore it shall be set equal to a reference value, j_0; consequently equation (5) is trivially satisfied. The remaining four equations are to be solved subject to

$$\bar{u} = \bar{v} = 0, \qquad \bar{N} = -n\bar{u}_{\bar{y}} \quad \text{on} \quad \bar{y} = 0, \tag{6}$$

and

$$\bar{u} \to U_0, \qquad \bar{v} \to 0, \quad \text{and} \quad \bar{N} \to 0 \quad \text{as} \quad \bar{y} \to \infty. \tag{7}$$

In equation (6) we have followed [4] by assigning a variable relation between $\bar{N}$ and the surface shear stress. The value $n = 0$ corresponds to the case where the particle density is sufficiently great that microelements close to the wall are unable to rotate. The value $n = \frac{1}{2}$ is indicative of weak concentrations, and when $n = 1$, we have flows which are representative of turbulent boundary layers (cf. [11]). We shall consider values of n which lie between these two extremes.

The above equations are nondimensionalized using the definitions

$$(\bar{u}, \bar{v}) = U_0(u, v), \qquad (\bar{x}, \bar{y}) = l(x, y),$$
$$\bar{p} = \rho U_0^2 p, \qquad \bar{t} = (l/U_0)t, \qquad \bar{N} = (U_0/l)N, \tag{8}$$

where $j_0 = l^2$ defines the lengthscale, l. We then obtain the following:

$$u_x + v_y = 0, \tag{9}$$

$$u_t + uu_x + vu_y = -p_x + \frac{K}{\mathrm{Re}}N_y + \left(\frac{1+K}{\mathrm{Re}}\right)(u_{xx} + u_{yy}), \tag{10}$$

$$v_t + uv_x + uv_y = -p_y - \frac{K}{\mathrm{Re}}N_x + \left(\frac{1+K}{\mathrm{Re}}\right)(v_{xx} + v_{yy}), \tag{11}$$

$$N_t + uN_x + vN_y = -\left(\frac{2K}{\mathrm{Re}}\right)N + \left(\frac{K}{\mathrm{Re}}\right)(v_x - u_y) + \left(\frac{1+\frac{K}{2}}{\mathrm{Re}}\right)(N_{xx} + N_{yy}), \tag{12}$$

and these equations need to be solved subject to the boundary conditions

$$u = v = 0, \qquad N = -nu_y \quad \text{on} \quad y = 0 \tag{13}$$

and

$$u \to 1, \qquad v \to 0, \quad \text{and} \quad N \to 0 \quad \text{as} \quad y \to \infty. \tag{14}$$

Here Re is the Reynolds number defined in the usual way and $K \equiv \kappa/\mu$.

We now invoke the boundary layer approximation by formally letting the Reynolds number become asymptotically large and setting

$$x = \mathrm{Re}\, X, \qquad y = Y, \qquad u = \psi_Y \quad \text{and} \quad v = -\mathrm{Re}^{-1}\psi_X \tag{15}$$

in equations (9)–(12). (It should be noted that we have taken x to be $O(\mathrm{Re})$ here. If we had assumed that x is substantially smaller than this, then it may be shown that the resulting boundary layer is always self-similar; this may be seen by taking a small-X expansion in the non-similar equations given later in (19) and (20). Within the $O(\mathrm{Re})$ range of values, the flow is generally nonsimilar, and therefore this range is the appropriate one to study.) Under the assumption that the flow is steady, the leading order equations for the streamfunction ψ and the gyration component N may be written as

$$\psi_X\psi_{XY} - \psi_X\psi_{YY} = (1+K)\psi_{YYY} + KN_Y, \tag{16}$$

$$\psi_Y N_X - \psi_X N_Y = -2KN - K\psi_{YY} + \left(1+\frac{K}{2}\right)N_{YY}. \tag{17}$$

The reduced streamfunction, f, the reduced gyration component, g, and the pseudo-similarity variable, η, are defined according to

$$\psi = X^{1/2}f(X,\eta), \qquad N = X^{-1/2}g(X,\eta), \qquad \eta = YX^{-1/2}, \tag{18}$$

and hence (16) and (17) become

$$(1+K)f''' + \tfrac{1}{2}ff'' + Kg' = X(f'f'_X - f''f_X), \tag{19}$$

$$\left(1+\frac{K}{2}\right)g'' + \frac{1}{2}(fg' + gf') = X(f'g_X - f_Xg') + KX(2g + f''), \tag{20}$$

where primes represent derivatives with respect to η. The boundary conditions are

$$f = f' = g + nf'' = 0 \quad \text{on} \quad \eta = 0; \quad f' \to 1, \; g \to 0 \quad \text{as} \quad \eta \to \infty. \tag{21}$$

Thus we have derived a set of parabolic partial differential equations which govern the development of the boundary layer and, in general, these require numerical solution.

Before presenting the computed results it is convenient to draw attention to two cases for which equations (19)–(21) admit similarity solutions. When $n = \frac{1}{2}$ we can set $f(X,\eta) = f_0(\eta)$ and $g(X,\eta) = g_0(\eta)$ where

$$\left(1+\frac{K}{2}\right)f_0''' + \frac{1}{2}f_0f_0'' = 0 \quad \text{and} \quad g_0 = -\frac{1}{2}f_0''. \tag{22}$$

This similarity solution can be written in terms of the standard Blasius boundary layer equations by simply rescaling the similarity variable. Thus

$$f_1(\eta) = \left(1+\frac{1}{2}K\right)^{1/2}\hat{f}(\hat{\eta}) \tag{23}$$

where $\eta = (1+\frac{1}{2}K)^{1/2}\hat{\eta}$, and $\hat{f}$ satisfies

$$\hat{f}_{\hat{\eta}\hat{\eta}\hat{\eta}} + \frac{1}{2}\hat{f}\hat{f}_{\hat{\eta}\hat{\eta}} = 0 \tag{24}$$

subject to

$$\hat{f}(0) = 0, \quad \hat{f}_{\hat{\eta}}(0) = 0 \quad \text{and} \quad \hat{f}_{\hat{\eta}} \to 1 \quad \text{as} \quad \hat{\eta} \to \infty. \tag{25}$$

A second similarity solution arises when $K = 0$ for which

$$f(\eta) = \hat{f}(\eta) \quad \text{and} \quad g(\eta) = -n\hat{f}''(0)\mathrm{e}^{-1/2\int_0^\eta \hat{f}(\xi)\,\mathrm{d}\xi}. \tag{26}$$

In this case the flow field is unaffected by the microstructure of the fluid and hence the gyration component is a passive quantity.

3. NUMERICAL SOLUTION

The full non-similar boundary-layer equations (19) and (20) were solved numerically using the Keller-box method. A nonuniform grid of 157 points was used in the η-direction with the grid points concentrated towards $\eta = 0$ in order to resolve adequately the developing near-wall layer mentioned previously. In the ξ-direction a nonuniform grid of 187 points was used and in all cases we chose $\xi_{max} = 100$ and $\eta_{max} = 100$; a larger value of ξ_{max} was found to result in a poorly resolved near-wall layer, whilst the value of η_{max} is well outside the main boundary layer. Newton–Raphson iteration at each streamwise station was used to solve the nonlinear difference equations, and convergence was deemed to have taken place when the maximum absolute pointwise change between successive iterates was 10^{-10}. Double precision arithmetic was used throughout.

In Fig. 1 we display profiles of the reduced gyration component, g, as a function of η at various streamwise locations X with the parameter choice $K = 0.5$ and the two cases $n = 0$ and $n = 1$. When $n = 0$ the value of g at $\eta = 0$ is zero, in accordance with the appropriate boundary condition in (21). On the other hand, the value of g at $\eta = 0$ when $n = 1$ varies with X. For both values of n, (and also for other values not equal to $\frac{1}{2}$), the g profile varies with increasing X. As

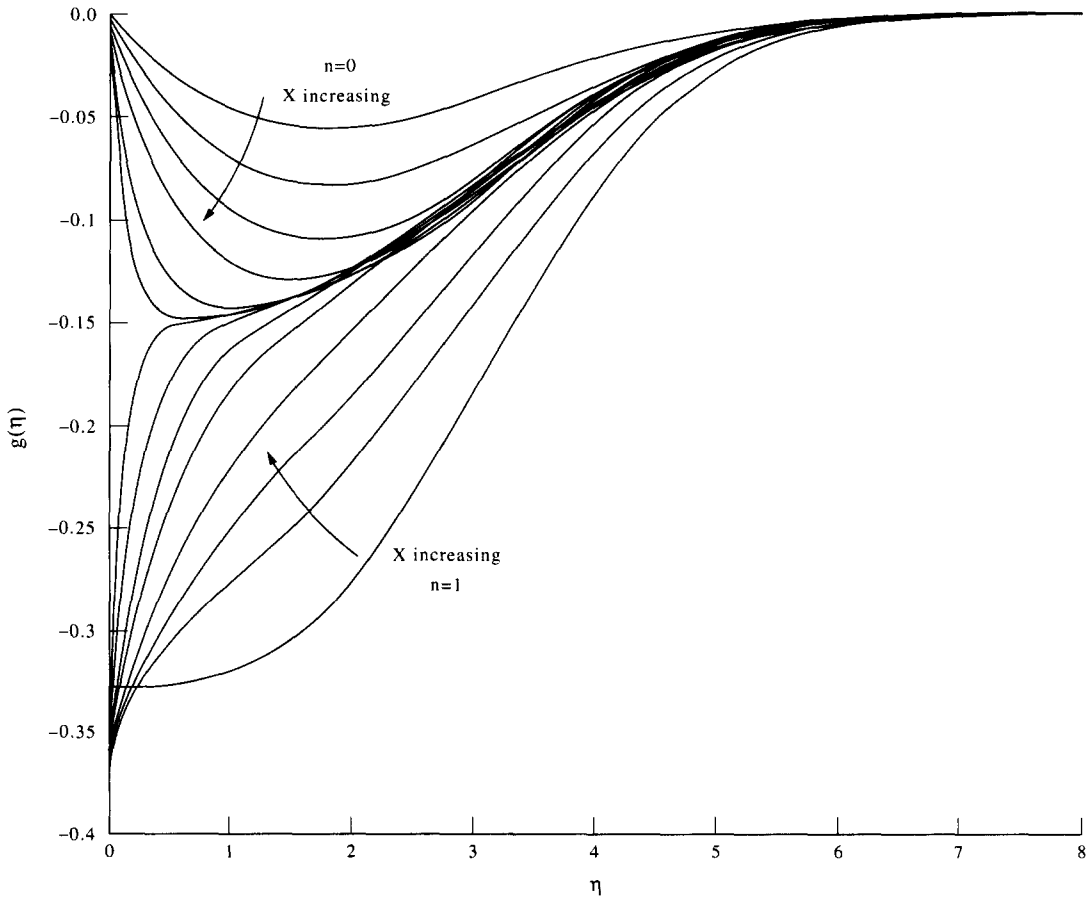

Fig. 1. Profiles of the reduced gyration component, g, as a function of η at different streamwise locations for $K = 0.5$ and for both $n = 0$ and $n = 1$. The values of X used are: $X = 0$, 0.5, 1.0, 2.0, 5.0, 10.0, 25.0 and 100.0.

X becomes large, g becomes independent of n and equal, in fact, to the $n = \frac{1}{2}$ similarity profile, in most of the main boundary layer. Deviations from the $n = \frac{1}{2}$ similarity profile can be seen to occur in an increasingly narrow region close to $\eta = 0$. An analysis of this sublayer is presented in the next section, and detailed results, including numerical comparisons, are given there.

It is difficult to show clearly the corresponding streamwise velocity profiles, f', on the same plot, and therefore these are presented separately in Figs 2(a) and (b), for $n = 0$ and $n = 1$, respectively. There seems to be very little variation in the velocity profiles as X increases. When $n < \frac{1}{2}$ the velocity at any one chosen value of η increases slightly as X increases, whereas it reduces when $n > \frac{1}{2}$.

Having seen the evolution of the velocity and gyration component profiles we now consider the variations of both the shear stress and of the rate of change of the gyration component at the solid boundary with X. In Figs 3(a) and (b) are shown f'' at $\eta = 0$ as a function of X for various values of K, and for $n = 0$ and $n = 1$, respectively. Larger initial variations of f'' would seem to be associated with increasingly large values of K, suggesting that the asymptotic results could be valid for fairly small values of X. In these figures, we have only shown the variation over the interval from $X = 0$ to $X = 2$; thereafter the curves are very close to being horizontal lines. The corresponding figures for the quantity, $g'(X, \eta = 0)X^{-1/2}$ are shown in Figs 4(a) and (b). The value of g' at the boundary is positive or negative depending on whether n is greater than or less than $\frac{1}{2}$, respectively. Again, as K increases, the approach to the steady state occurs at decreasing distances from the leading edge. The values of this function at $X = 100$ will be compared later with the results of an asymptotic analysis in the next section.

In Figs 3 and 4 we considered a range of values of K with n fixed. We now present the corresponding graphs where $K = 0.5$ is taken, and n is varied between 0 and 1; these appear as Figs 5 and 6, respectively. The similarity solution corresponding to $n = 0.5$ is evident as a straight line in both these figures.

4. ASYMPTOTIC SOLUTION

We turn our attention now to the solution of equations (19) and (20) at increasingly large distances downstream of the leading edge.

When X is very large a simple order-of-magnitude analysis of equation (20) indicates that the final term is much larger than all the others if η is $O(1)$, unless the coefficient of X, $2g + f_{\eta\eta}$, is zero. That this is indeed the case is supported by the graphical evidence of Fig. 7, which shows successive profiles of $(g + f''/2)$ as a function of η at increasing values of X. Of interest now is the behaviour of this function near $\eta = 0$ as X increases and Fig. 7 shows the development of a near-wall layer of decreasing thickness. It is straightforward to check that setting $g = -\frac{1}{2}f''$ in (19) and (20) yields a consistent pair of equations and f is then given by the solution of

$$\left(1 + \frac{K}{2}\right)f''' + \frac{1}{2}ff'' = X(f'f'_X - f''f_X). \tag{27}$$

However, the boundary condition for g, now set equal to $-\frac{1}{2}f''$, is not satisfied unless $n = \frac{1}{2}$. This suggests that for $n \neq \frac{1}{2}$ a narrow layer forms near $\eta = 0$ which allows the transition between an "outer" solution (which is the similarity solution (22) corresponding to $n = \frac{1}{2}$) and an "inner" solution which is required in order to satisfy the correct boundary conditions; again this conjecture is supported by Fig. 7. In this near-wall layer g cannot be equal to $-\frac{1}{2}f''$ and hence the final term in the right-hand side of (20) must be large. The only means of balancing a term of this size is to assume that g'' is as large, which it will be if η is sufficiently small. Hence if

$$\left(1 + \frac{1}{2}K'\right)g'' \sim KX(2g + f'') \tag{28}$$

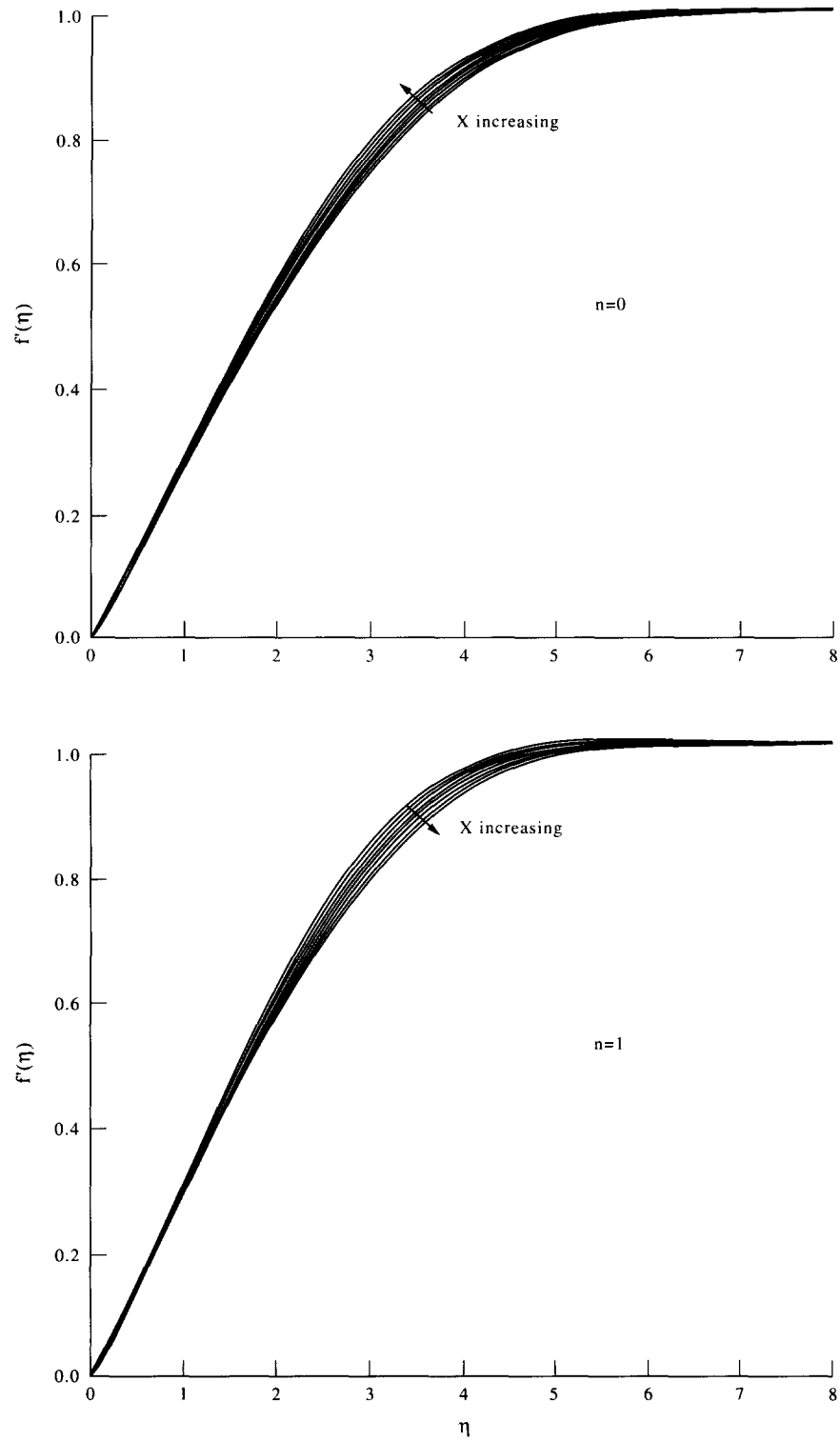

Fig. 2. Profiles of the reduced streamwise velocity, f', as a function of η at different streamwise locations for $K = 0.5$ and for both $n = 0$ and $n = 1$. The values of X used are as given in Fig. 1.

for large values of X, then $\eta = O(X^{-1/2})$ defines the depth of the near wall layer. Within this region, wherein we assume that the coordinate, ζ, defined by

$$\zeta = \eta X^{1/2}, \tag{29}$$

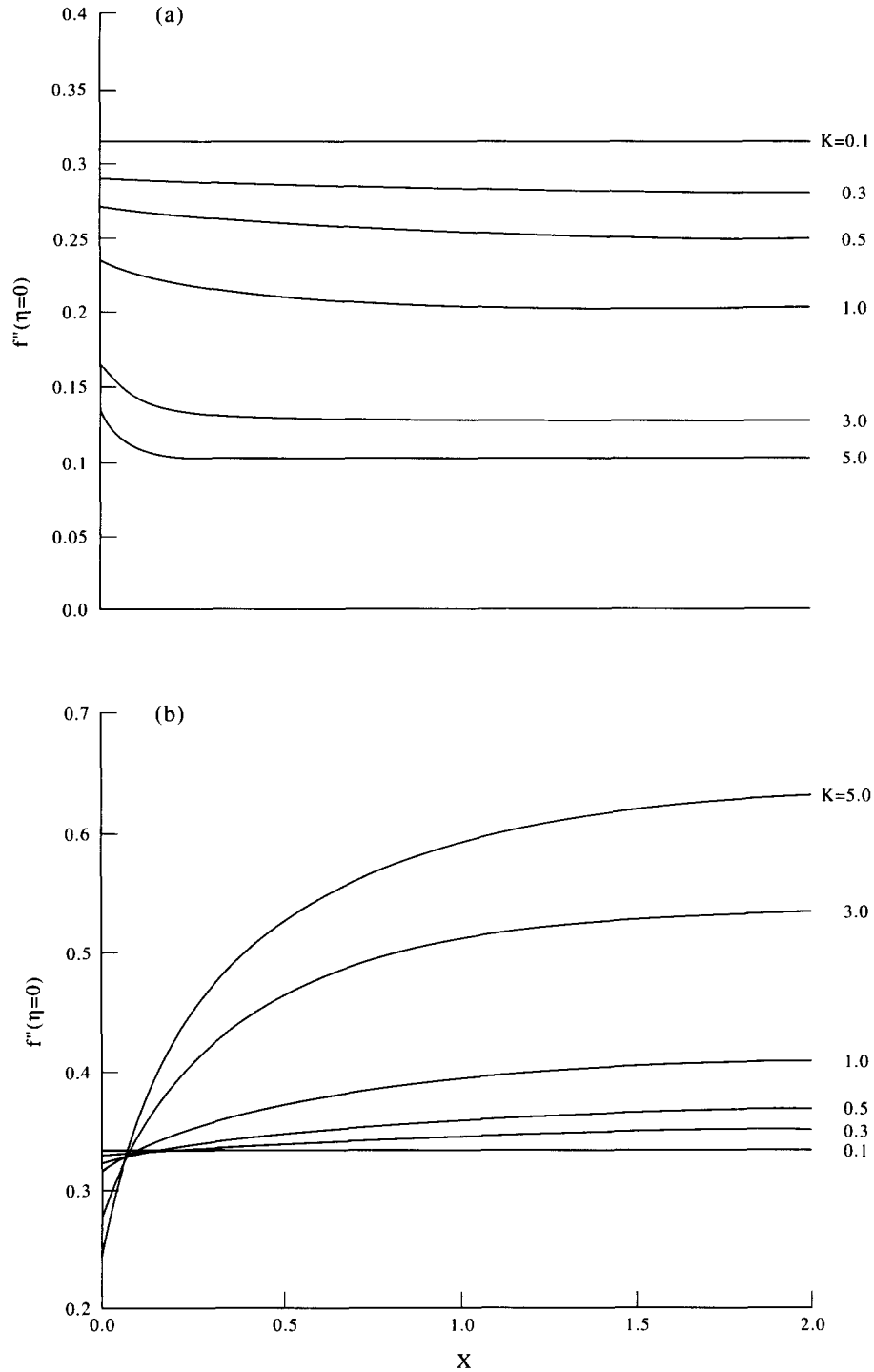

Fig. 3. Development of the wall shear stress $f''(X, \eta = 0)$, as a function of X for (a) $n = 0$ and (b) $n = 1$, and for various values of K.

is $O(1)$ as $X \to \infty$, the $n = \frac{1}{2}$ solution given by (22) expands as

$$f_0 = -X^{-1}\zeta^2 g_0(0) + \ldots . \tag{30}$$

Using the argument presented above we anticipate that within this near-wall layer the

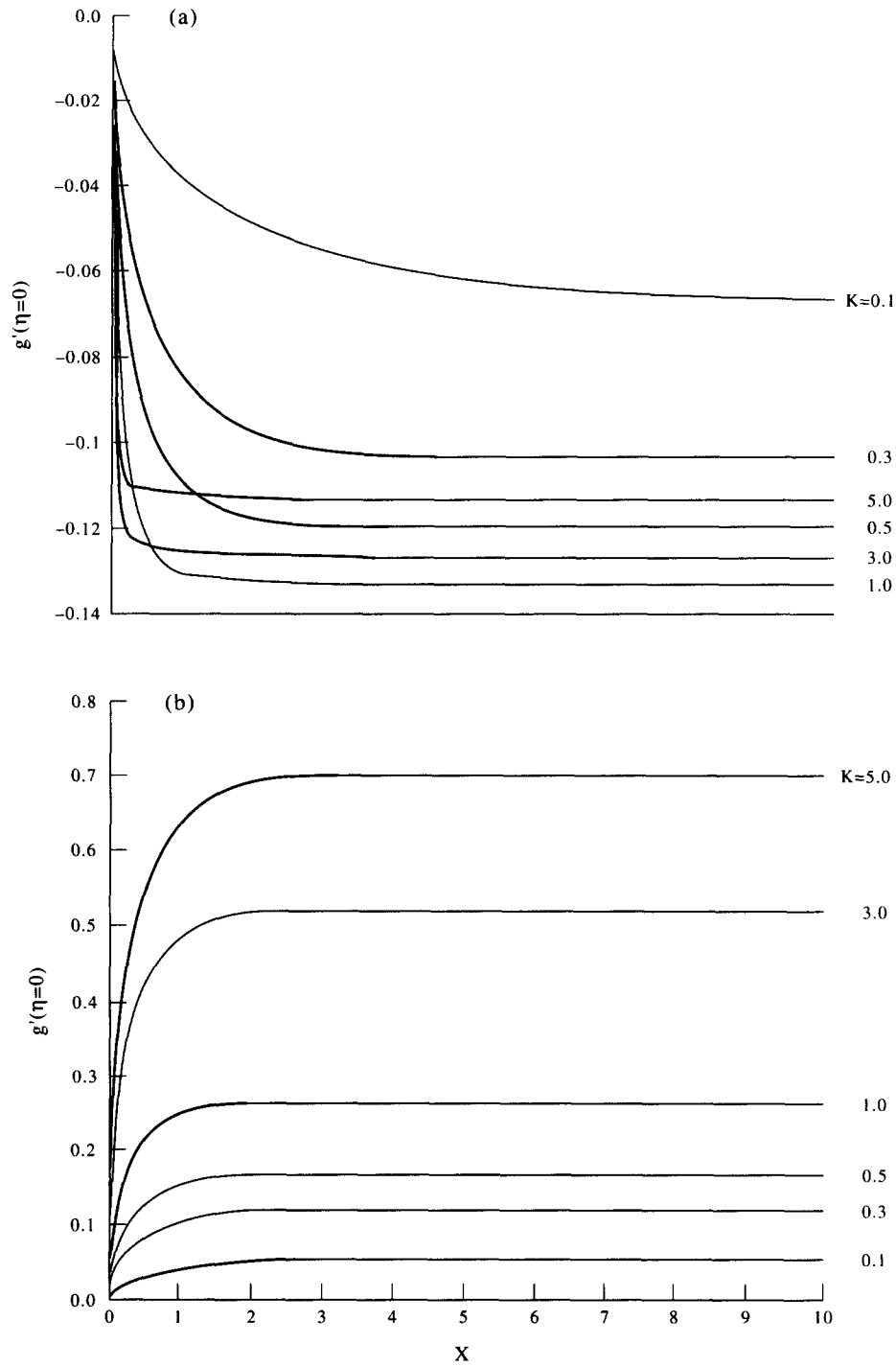

Fig. 4. Development of the rate of change of the gyration component at the wall, $g'(X, \eta = 0)$, as a function of X for (a) $n = 0$ and (b) $n = 1$, and for various values of K.

solutions, $f(X, \eta)$ and $g(X, \eta)$ are perturbed from the $n = \frac{1}{2}$ case. Therefore when $n \neq \frac{1}{2}$ we seek solutions with the form,

$$f(X, \eta) = X^{-1}[-\zeta^2 g_0(0) + f_1(\zeta)] + O(X^{-3/2}),$$
$$g(X, \eta) = g_0(0) + g_1(\zeta) + O(X^{-1/2}). \tag{31}$$

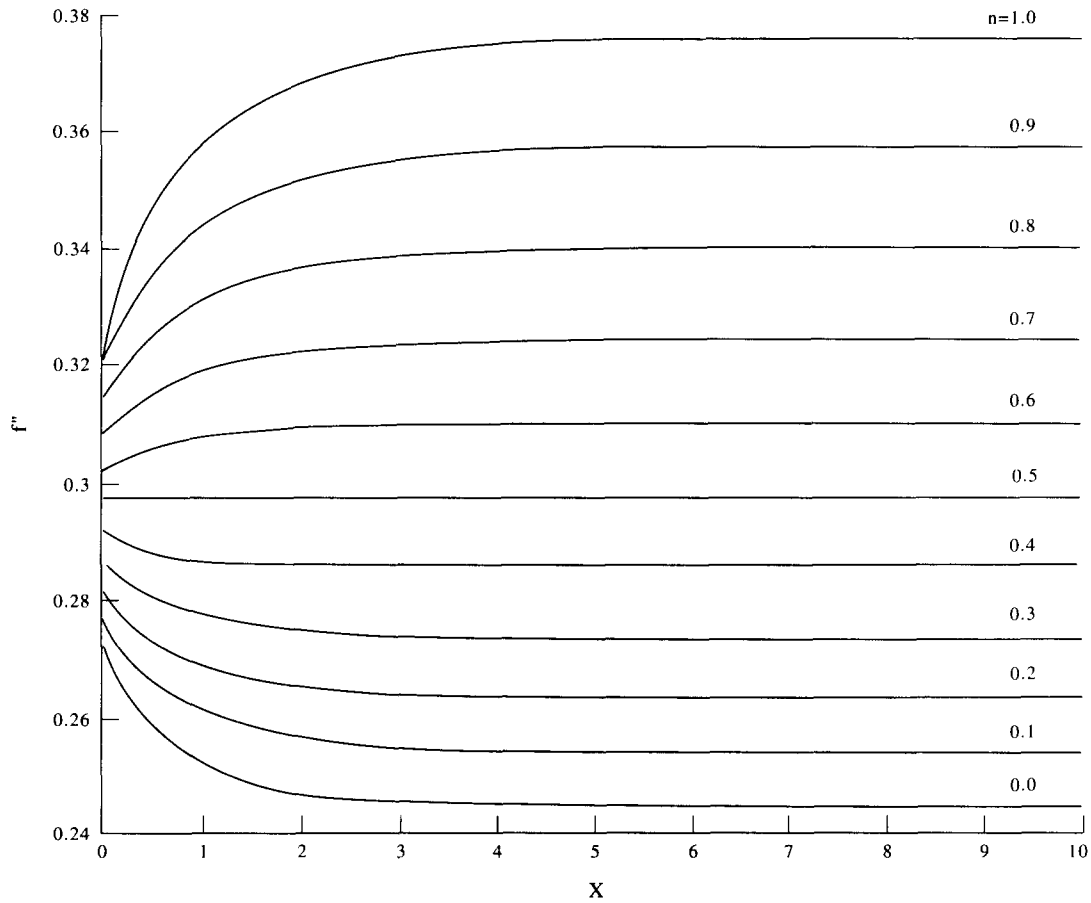

Fig. 5. Development of the wall shear stress $f''(X, \eta = 0)$ as a function of X for $K = 0.5$ and a range of values of n.

Substitution of these forms into (19)–(21), suitably modified by means of the transformation (29), yields the equations

$$(1 + K)f_{1\zeta\zeta\zeta} + Kg_{1\zeta} = 0, \tag{32}$$

$$\left(1 + \frac{1}{2}K\right)g_{1\zeta\zeta} = K(2g_1 + f_{1\zeta\zeta}), \tag{33}$$

at leading order. The appropriate boundary conditions for f_1 and g_1 are:

$$f_1(0) = 0, \quad f_{1\zeta} = 0, \quad g_1(0) + nf_{1\zeta\zeta}(0) = (2n - 1)g_0(0), \tag{34}$$

and

$$f_{1\zeta\zeta}, g_1 \to 0 \quad \text{as} \quad \zeta \to \infty. \tag{35}$$

It is necessary to point out that we have set $f_{1\zeta\zeta}$, rather than $f_{1\zeta}$ to tend to zero as $\zeta \to \infty$. The reason is simply that $f_{1\zeta} \to 0$ is too restrictive, and that if $f_{1\zeta} \to$ constant then the perturbations to f_0 in (27) is still asymptotically small in the main boundary layer. This small perturbation will eventually contribute to a second-order, that is an $O(X^{-1/2})$, correction to the leading order main-layer solution denoted by the zero subscript and satisfying (22).

It is straightforward to show that equations (32) and (33) subject to the boundary conditions (34) and (35) are satisfied by the solutions

$$f_1 = A[1 - \lambda\zeta - e^{-\lambda\zeta}], \tag{36}$$

$$g_1 = 2Ae^{-\lambda\zeta}, \tag{37}$$

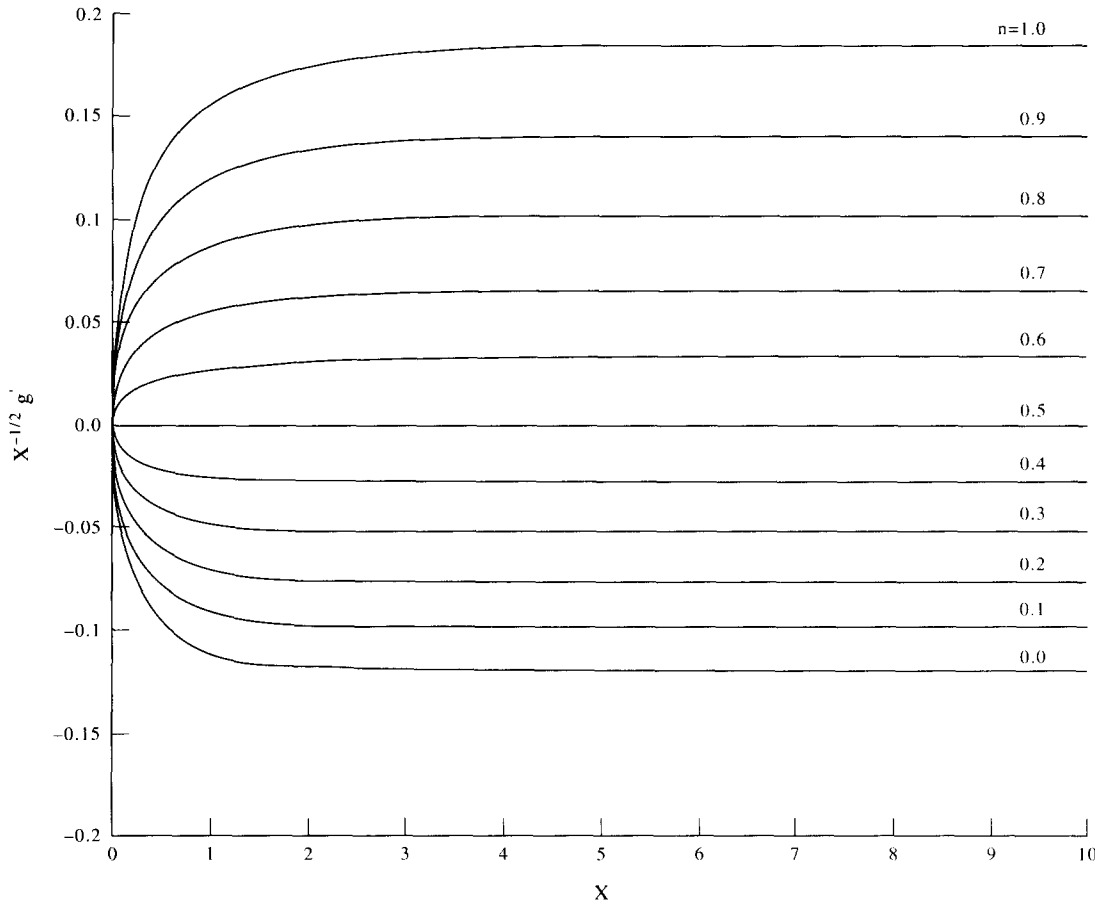

Fig. 6. Development of the function, $X^{-1/2}g'(X, \eta = 0)$, as a function of X for $K = 0.5$ and a range of values of n.

where

$$A = \frac{(2n-1)(K+1)g_0(0)}{2[1+(1-n)K]} \quad \text{and} \quad \lambda = \left(\frac{2K}{1+K}\right)^{1/2}. \tag{38a,b}$$

From (38b) we see that the near-wall layer has a thickness which depends only on the value of K, and not on n. Its thickness decreases as K increases, but tends to a constant as K increases indefinitely.

5. CONCLUSION

A wide selection of numerical results have been presented giving the evolution of the velocity and gyration component profiles, and the shear stress and rate of change of gyration component at the solid surface. These numerical results have indicated that a near-wall contact layer develops as $X \to \infty$ but only if $n \neq \frac{1}{2}$. An asymptotic analysis has shown that this inner layer has thickness of magnitude $O(X^{-1/2})$ in terms of η, or, alternatively, of magnitude $O(1)$ in terms of Y (see equation (17c)). When either $n = \frac{1}{2}$ or $K = 0$ the solution is self-similar and there is no near-wall layer.

The easiest quantity which we can use to compare the numerical and symptotic results is

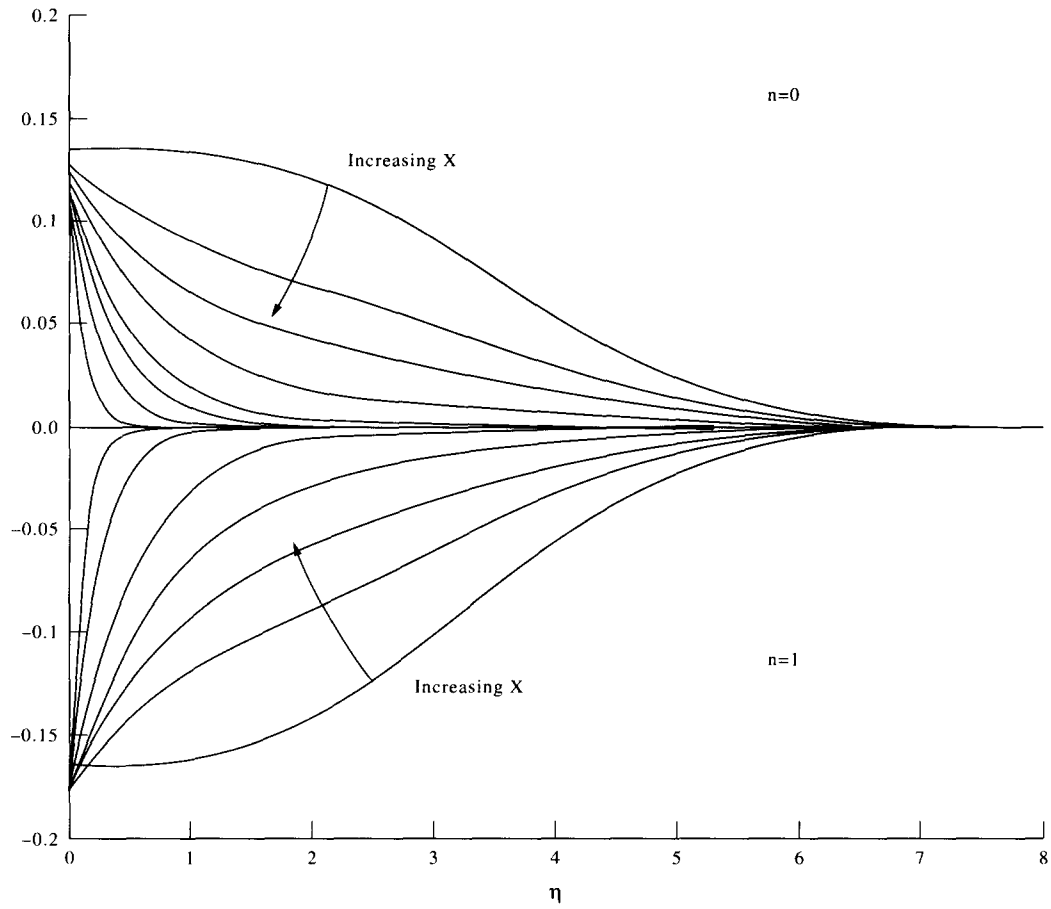

Fig. 7. Profiles of the function, $g + \frac{1}{2}f''$, as a function of η at different streamwise locations for $K = 0.5$ and for both $n = 0$ and $n = 1$. The values of X used are as given in Fig. 1. This figure demonstrates (i) the diminishing size of the developing near-wall layer, and (ii) the approach to $g = -\frac{1}{2}f''$ outside the near-wall layer, as X increases.

$g_\eta(0)$. Using (23), (29), (31), (37) and (38), it is possible to show that

$$g_\eta(\eta = 0) \sim \left[\frac{K(1+K)}{2+K}\right]^{1/2} \frac{(2n-1)\hat{f}_{\hat{\eta}\hat{\eta}}(0)}{[1+(1-n)K]} X^{1/2}, \tag{39}$$

as $X \to \infty$, where $\hat{f}_{\hat{\eta}\hat{\eta}}(0) = 0.3321$. In Figs 4 and 6 we have shown some graphs of the behaviour of $X^{-1/2}g_\eta$ $(\eta = 0)$ as a function of X. According to the theory of the last section, resulting in (39), this function should asymptote to a constant as $X \to \infty$. These figures demonstrate that

Table 1. Comparison of numerical and asymptotic values of $X^{-1/2}g_\eta$ at $X = 100$ and $\eta = 0$ for $n = 0$ and different values of K. Asymptotic values were obtained using equation (39)

K	Numerical	Asymptotic
0.1	−0.06895	−0.06906
0.3	−0.1050	−0.1051
0.5	−0.1211	−0.1212
1.0	−0.1354	−0.1355
3.0	−0.1285	−0.1285
5.0	−0.1145	−0.1145

this is indeed the case, and further, that the approach to the asymptotic value takes place increasingly quickly as K increases. Table 1 compares values obtained numerically at a value of $X = 100$ and those given by (39); the agreement is seen to be extremely good. Another quantity of interest is the fluid shear stress at the solid surface. It may be shown that

$$f_{\eta\eta} \sim \frac{(1 + \frac{1}{2}K)^{1/2}\hat{f}_{\hat{\eta}\hat{\eta}}(0)}{[1 + (1 - n)K]}, \tag{40}$$

as $X \to \infty$, thereby indicating that the shear stress is affected by the presence of microrotational effects and varies with both K and n.

REFERENCES

[1] A. C. ERINGEN, *J. Math. Mech.* **16,** 1 (1966).
[2] R. S. R. GORLA, *Int. J. Engng Sci.* **27,** 77 (1989).
[3] R. S. R. GORLA, *Int. J. Engng Sci.* **26,** 883 (1988).
[4] R. S. R. GORLA, *Int. J. Engng Sci.* **30,** 349 (1992).
[5] A. A. ARAFA and R. S. R. GORLA, *Int. J. Engng Sci.* **30,** 1745 (1992).
[6] C.-P. CHIU and H.-M. CHOU, *Acta Mechanica* **101,** 161 (1993).
[7] K. UNSWORTH and T. C. CHIAM, *ZAMM* **61,** 463 (1981).
[8] G. AHMADI, *Int. J. Engng Sci.* **14,** 639 (1976).
[9] R. S. AGARWAL and C. DHANAPAL, *Int. J. Engng Sci.* **26,** 1257 (1988).
[10] T.-Y. WANG and C. KLEINSTREUER, *Int. J. Engng Sci.* **26,** 1267 (1988).
[11] J. PEDDIESON Jr, *Int. J. Engng Sci.* **10,** 23 (1972).
[12] H. B. KELLER, *A. Rev. Fluid Mech.* **10,** 417 (1978).

(Received 7 September 1994; accepted 7 June 1995)

NOMENCLATURE

A = constant used in equations (36)–(38)
f = reduced streamfunction
f_0 = reduced streamfunction for $n = \frac{1}{2}$
f_1 = perturbation to the reduced streamfunction in the near-wall layer
$\hat{f}$ = reduced streamfunction for the classical Blasius boundary-layer flow
g = reduced gyration component
g_0 = reduced gyration component for $n = \frac{1}{2}$
g_1 = perturbation to the reduced gyration component in the near-wall layer
j = microinertia density
j_0 = reference value of the microinertia density
K = ratio of the gyroviscosity and the fluid viscosity
l = length scale
n = ratio of the gyration vector component and the fluid shear at a solid boundary
N = the gyration vector component perpendicular to the x–y plane
p = pressure
Re = Reynolds number, $\rho U_0 l/\mu$
t = time
u,v = fluid velocities in the x and y directions, respectively
U_0 = free stream velocity
x,y = streamwise and cross-stream Cartesian coordinates
X,Y = nondimensional streamwise and cross-stream Cartesian coordinates

Greek symbols

η = pseudo-similarity variable
$\hat{\eta}$ = scaled pseudo-similarity variable
γ = spin-gradient viscosity
μ = dynamic viscosity
κ = coefficient of gyroviscosity
λ = constant used in equations (36)–(38)
ρ = density
ψ = streamfunction
ζ = scaled pseudo-similarity variable

Superscripts

$'$ = differentiation with respect to η
$^-$ = dimensional variables

Subscripts

X = differentiation with respect to X
Y = differentiation with respect to Y
ζ = differentiation with respect to ζ